Controlling the Interparticle Spacing of Au−Salt Loaded Micelles and Au Nanoparticles on Flat Surfaces

ARTICLE *in* LANGMUIR · OCTOBER 2007

Impact Factor: 4.46 · DOI: 10.1021/la7012304 · Source: PubMed

8 AUTHORS, INCLUDING:

Joachim Bansmann
Universität Ulm
113 PUBLICATIONS **1,909** CITATIONS
SEE PROFILE

Harry E Hoster
Lancaster University
96 PUBLICATIONS **2,236** CITATIONS
SEE PROFILE

Ulf Wiedwald
University of Duisburg-Essen
70 PUBLICATIONS **1,044** CITATIONS
SEE PROFILE

Controlling the Interparticle Spacing of Au−Salt Loaded Micelles and Au Nanoparticles on Flat Surfaces

J. Bansmann,*,† S. Kielbassa,† H. Hoster,† F. Weigl,‡ H. G. Boyen,‡,§ U. Wiedwald,‡ P. Ziemann,‡ and R. J. Behm*,†

Institute of Surface Chemistry and Catalysis, Ulm University, D-89069 Ulm, Germany, and Institute of Solid State Physics, Ulm University, D-89069 Ulm, Germany

Received April 27, 2007. In Final Form: July 13, 2007

The self-organization of diblock copolymers into micellar structures in an appropriate solvent allows the deposition of well ordered arrays of pure metal and alloy nanoparticles on flat surfaces with narrow distributions in particle size and interparticle spacing. Here we investigated the influence of the materials (substrate and polymer) and deposition parameters (temperature and emersion velocity) on the deposition of metal salt loaded micelles by dip-coating from solution and on the order and inter-particle spacing of the micellar deposits and thus of the metal nanoparticle arrays resulting after plasma removal of the polymer shell. For identical substrate and polymer, variation of the process parameters temperature and emersion velocity enables the controlled modification of the interparticle distance within a certain length regime. Moreover, also the degree of hexagonal order of the final array depends sensitively on these parameters.

1. Introduction

Nanostructured surfaces consisting of size-controlled metal nanoparticles on a planar substrate are highly interesting model systems for fundamental research on physical and chemical processes such as optical,[1] magnetic,[2,3] or catalytic[4−7] properties. This is even more the case if, in addition to a narrow distribution in particle sizes, also the interparticle spacing can be controlled independently with a narrow distribution of interparticle distances. For example, magnetic phenomena of nanoscaled materials and catalytic reactions are just two areas where the desired properties may not only depend on the size of the individual nanostructures but also on their spacing, due to dipolar magnetic interactions between neighboring particles[8,9] or due to spill-over and transport processes on the surface. A preparation technique that provides for variable distances with a narrow distribution of inter-particle separations without modifying the particles themselves would thus be highly interesting for studying the influence of such interactions and effects as a function of the distance. Among the various methods applied for depositing metal nanoparticles on planar surfaces, which range from deposition of single atoms and their subsequent coalescence into nanoparticles[10] via deposition of preformed nanoparticles such as ligand-stabilized nanoparticles,[11−14] mass-selected clusters,[15−17]or metal-loaded micelles[18,19] finally to lithographic methods such as electron beam lithography[20] or colloidal lithography,[21−24] only few techniques allow for a controlled, nonstatistical nanoparticle deposition with narrow interparticle separations. Examples include the preferential nucleation and growth of nanoparticles on regular surface inhomogeneities, which are provided, e.g., by reconstructed surfaces such as the herringbone reconstruction of Au(111),[25,26] or by template adlayers[16,17]as bottom-up approach or, on the other hand, electron beam deposition as top-down approach. One of the very few techniques, if not the only one, which allows nanostructured surfaces to be produced with both a very narrow size distribution of the nanostructures and a narrow distribution

* Authors to whom correspondence should be addressed. E-mail: joachim.bansmann@uni-ulm.de; juergen.behm@uni-ulm.de.

† Institute of Surface Chemistry and Catalysis.

‡ Institute of Solid State Physics.

§ Present address: Institute of Materials Research (IMO), University of Hasselt, Wetenschapspark 1, B-3590 Diepenbeek, Belgium.

(1) Kreibig, U. *Optical Properties of Metal Clusters*; Springer-Verlag: Berlin, 1995.

(2) Bansmann, J.; Baker, S. H.; Binns, C.; Blackman, J. A.; Bucher, J. P.; Dorantes-Dávila, J.; Dupuis, V.; Favre, L.; Kechrakos, D.; Kleibert, A.; Meiwes-Broer, K.-H.; Pastor, G. M.; Perez, A.; Toulemonde, O.; Trohidou, K. N.; Tuaillon, J.; Xie, Y. *Surf. Sci. Rep.* **2007**, *56*, 189.

(3) Sellmyer, D.; Skomski, R. *Advanced Magnetic Nanostructures*; Springer-Verlag: Berlin, 2006.

(4) Rainer, D. R.; Goodman, D. W. *J. Mol. Catal.* **1997**, *131*, 259.

(5) *Chemisorption and Reactivity on Supported Clusters and Thin Films*; Lambert, R. M., Pacchioni, G., Eds.; Kluwer Academic Publishers: Dordrecht, The Netherlands, 1997.

(6) Henry, C. R. *Surf. Sci. Rep.* **1998**, *31*, 231.

(7) Freund, H. J. *Surf. Sci.* **2002**, *500*, 271.

(8) Zeng, H.; Sun, S.; Vedantam, T. S.; Liu, J. P.; Dai, Z. R.; Wang, Z. L. *Appl. Phys. Lett.* **2002**, *80*, 2583.

(9) Puntes, V. F.; Gorostiza, P.; Aruguete, D. M.; Bastus, N. G.; Alivisatos, A. P. *Nat. Mater.* **2004**, *3*, 263.

(10) Venables J. A.; Spiller, G. D. T. *Surface Diffusion on Solid Materials*; Plenum Press: New York, 1982; pp 1−64.

(11) Schmidt, T. J.; Noeske, M.; Gasteiger, H. A.; Behm, R. J.; Britz, P.; Brijoux, W.; Bönnemann, H. *J. Electrochem. Soc.* **1998** *145*, 925.

(12) Maye, M. M.; Lou, Y.; Zhong, C.-J. *Adv. Mater.* **2001**, *13*, 1507.

(13) Chusuei, C. C.; Lai, K.; Davis, K. A.; Bowers, E. K.; Fackler, J. P.; Goodman, D. W. *Langmuir* **2001**, *17*, 4113.

(14) Link, S.; El-Sayed, M. A.; Schaaf, T. G.; Whetten, R. L. *Chem. Phys. Lett.* **2002**, *356*, 240.

(15) Meiwes-Broer, K.-H. *Metal Clusters on Surfaces*; Springer-Verlag: Berlin, 2000.

(16) Queitsch, U.; Mohn, E.; Schäffel, F.; Schultz, L.; Rellinghaus, B.; Blüher, A.; Mertig, M. *Appl. Phys. Lett.* **2007**, *90*, 113114.

(17) Terheiden, A.; Mayer, C.; Moh, K.; Stahlmecke, B.; Stappert, S.; Acet, M.; Rellinghaus, B. *Appl. Phys. Lett.* **2004**, *84*, 3891.

(18) Spatz, J.; Mossmer, S.; Möller, M.; Herzog, T.; Plettl A.; Ziemann, P. *J. Lumin.* **1998**, *76−77*, 168.

(19) Kästle, G.; Boyen, H.-G.; Weigl, F.; Ziemann, P.; Riethmüller, S.; Hartmann, C.; Spatz, J. P.; Möller, M. M.; Garnier, M. G.; Oelhafen, P. *Phase Transitions* **2003**, *310*, 307.

(20) Tennant D. M. *Nanotechnology*; Springer-Verlag: New York, 1998; p 161.

(21) Burmeister, F.; Schäfle, C.; Mattes, T.; Böhmisch, M.; Boneberg, J.; Leiderer, P. *Langmuir* **1997**, *13*, 2983.

(22) Gunnarsson, L.; Bjerneld, E. J.; Xu, H.; Petronis, S.; Kasemo, B.; Käll, M. *Appl. Phys. Lett.* **2001**, *78*, 802−804.

(23) Werdinius, C.; Oesterlund, L.; Kasemo, B. *Langmuir* **2003**, *19*, 458−468.

(24) Österlund, L.; Kielbassa, S.; Werdinius, C.; Kasemo, B. *J. Catal.* **2003**, *215*, 94.

(25) Chambliss, D. D.; Wilson, R. J.; Chiang, S. *Phys. Rev. Lett.* **1991**, *66*, 1721−1724.

(26) Meyer, J. A.; Baikie, I. D.; Kopatzki, E.; Behm, R. J. *Surf. Sci.* **1996**, *365*, L647.

10.1021/la7012304 CCC: $37.00
Published on Web 08/28/2007

of interparticle spacings, is based on the micellar technique,[18,27,28] where nanoparticles are generated from chemical precursors such as metal salts loaded into the core of diblock−copolymer reverse micelles. After removing of the polymer shell in an appropriate plasma, metal nanoparticles are formed with a narrow size distribution and well-defined interparticle distances. Both parameters, the size and the distance between individual particles, can be controlled independently by choosing the appropriate polymers and metal salt loading.

This method, which is able to generate pure metal and alloy particles with sizes between 1 and 15 nm, has been applied to various areas in fundamental research, e.g., to magnetism of nanoparticles,[29−31] to catalytic reactions,[32−34] and even to a concept of fabricating densely packed arrays of diamond field emitters[35] via lithographic techniques. Although this technique has been investigated and applied for several years by different groups,[18,27,28,36−39] basic questions on the mechanism of the deposition process are still open. Although in a simple model the adsorbed micelles are assumed to be in direct contact, a number of experimental results indicate that also experimental parameters such as emersion velocity or temperature play a role (see also ref 40). This is the topic of the present study, where we investigated the influence of the emersion speed and process temperature on the deposition characteristics, in particular on the order and interparticle spacing in the mono-micellar films (thickness corresponding to one micelle), upon deposition of Au-salt loaded micelles on single crystalline TiO_2(110) substrates and oxidized silicon wafers.

2. Experimental Section

Rutile TiO_2(110) substrates (TBL Kelpin, Germany, one side polished, tolerance of the surface orientation <0.5°) were cleaned by first dipping in acetone (5 min in a supersonic bath) then in a H_2O_2/H_2SO_4 mixture (1:1) for 10 min and finally rinsing in Millipore water. Afterward, the samples were calcined in air for 1−2 h in an oven at 950 °C and then cooled down in air. This treatment leads to fully oxidized flat sample surfaces with broad terraces (50−200 nm), separated by monatomic steps.[41] Silicon wafers (100 oriented, Crystec) were used as received, with a cover layer of native silicon oxide (thickness typically 2−3 nm).

Gold nanoparticles were deposited onto the corresponding substrates by a micellar technique which was described in detail elsewhere.[18,27,28] Briefly, polystyrene [PS]−*block*-poly-[2-vinylpyridine] (P2VP) diblock copolymers are dissolved in toluene, where they self-assemble into spherical reverse micelles during careful stirring, with the hydrophilic P2VP part forming the micellar core and the hydrophobic PS part forming the outer shell. The notation PS[*x*]-*b*-P2VP[*y*] refers to the numbers of monomer units *x* and *y* of the respective polymers. In the present study, we mainly used PS^{528}-*b*-$P2VP^{177}$ diblock copolymers (Polymer Source, Inc.) for the preparation of Au loaded micelles on TiO_2(110). Next, the metal salt $HAuCl_4$ is added to the solution, which is accumulated in the micellar cores. After carefully stirring, all micelles are loaded with an equal amount of metal salt. The Au-salt loaded micelles are transferred onto the substrates by dipping the sample into the solution, followed by removing the substrate at a constant emersion velocity and at a controlled, constant temperature, in most cases at 20 °C. This procedure results in mono-micellar films with a high degree of hexagonal order. As a final step in order to prepare metal nanoparticles, the surrounding polymer is removed in oxygen plasma (RF-plasma, power 50 W, $p(O_2) = 4 \times 10^{-2}$ mbar, 30 min at 200 °C). The final result is an array of well-separated metallic particles of rather uniform size,[28] which show a high degree of hexagonal order. Details on the structural characterization and chemical state of Au/TiO_2 can be found in ref 33. After the plasma treatment, the samples were transferred in ambient conditions for imaging in a scanning electron microscope (SEM, Hitachi, imaging conditions 25 kV, 100k magnification).

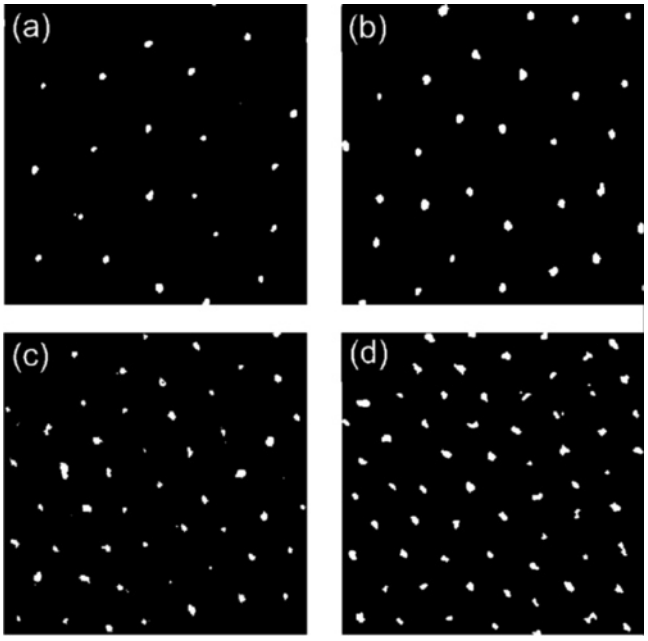

Figure 1. SEM images taken from ordered Au nanoparticles on TiO_2(110). The dip-coating velocity during deposition at 20 °C of the micelles has been varied: (a) 10, (b) 20, (c) 30, and (d) 40 mm min^{-1}. All images have identical scale (300 nm × 300 nm).

For a quantitative evaluation of the interparticle distances in the SEM and AFM images, we calculated the pair correlation functions for individual images. For the analysis of the particle distributions, the coordinates of the particle centers were determined. The pair correlation function $g(r)$ was calculated via the average probability $p(r)$ to find a second center in the radial range $(r, r + \Delta r)$ around a first one, divided by a factor $2\pi r$. $g(r)$ is then given by $g(r) = p(r)\rho^{-1}$, with ρ denoting the average surface density of particles. This ensures that $g(r) = 1$ for large r.

3. Results and Discussion

Figure 1 shows SEM images of the resulting Au nanoparticle arrays on the titania surface for dip-coating velocities between 10 (a) and 40 mm min^{-1} (d), with the white dots representing the Au nanoparticles. Although, due to the low conductivity of

(27) Spatz, J. P.; Mössmer, S.; Hartmann, C.; Möller, M.; Herzog, T.; Krieger, M.; Boyen, H.-G.; Ziemann, P.; Kabius, B. *Langmuir* **2000**, *16*, 407.
(28) Kästle, G.; Boyen, H.-G.; Weigl, F.; Lengl, G.; Herzog, Th.; Ziemann, P.; Riethmüller, S.; Meyer, O.; Hartmann, C.; Spatz, J.; Möller, M. M.; Ozawa, M.; Banhart, F.; Garnier, G.; Oelhafen, P. *Adv. Funct. Mater.* **2003**, *13*, 853.
(29) Boyen, H.-G.; Kästle, G.; Zürn, K.; Herzog, T.; Weigl, F.; Ziemann, P.; Mayer, O.; Jerome, C.; Möller, M.; Spatz, J.; Garnier, M. G.; Oelhafen, P. *Adv. Funct. Mater.* **2003**, *13*, 359.
(30) Ethirajan, A.; Wiedwald, U.; Boyen, H.-G.; Kern, B.; Han, L.; Klimmer, A.; Weigl, F.; Kästle, G.; Ziemann, P.; Fauth, K.; Cai, J.; Behm, R. J.; Oelhafen, P.; Walther, P.; Biskupek, J.; Kaiser, U. *Adv. Mater.* **2007**, *19*, 406.
(31) Wiedwald, U.; Klimmer, A.; Kern, B.; Han, L.; Boyen, H.-G.; Fauth, K.; Ziemann, P. *Appl. Phys. Lett.* **2007**, *90*, 062508.
(32) Roldan Cuenya, B.; Baeck, S. H.; Jaramillo, D. M.; McFarland, E. W. *J. Am. Chem. Soc.* **2003**, *125*, 12928.
(33) Kielbassa, S.; Häbich, A.; Schnaidt, J.; Bansmann, J.; Weigl, F.; Boyen, H.-G. A.; Ziemann, P.; Behm, R. J. *Langmuir* **2006**, *22*, 7873.
(34) Ono, L. K.; Sudfeld, D.; Cuenya, B. R. *Surf. Sci.* **2006**, *600*, 5041.
(35) Weigl, F.; Fricker, S.; Boyen, H.-G.; Dietrich, C.; Koslowski, B.; Plettl A.; Pursche, O.; Ziemann, P.; Walther, P.; Hartmann, C.; Ott, M.; Möller, M. *Diamond Relat. Mater.* **2006**, *15*, 1689.
(36) Krischnamoorthy, S.; Pugin, R.; Brugger, J.; Heinzelmann, H.; Hinderling, C. *Adv. Funct. Mater.* **2006**, *16*, 1429.
(37) Krischnamoorthy, S.; Pugin, R.; Brugger, J.; Heinzelmann, H.; Hoogerwerf, A. C.; Hinderling, C. *Langmuir* **2006**, *22*, 3450.
(38) Naitabdi, A.; Ono, L. K.; Roldan Cuenya, B. *Appl. Phys. Lett.* **2006**, *89*, 043101.
(39) Dietrich, C.; Koslowski, B.; Weigl, F.; Ziemann, P. *Surf. Interface Anal.* **2006**, *38*, 1034.
(40) Meiners, J. C.; Quintl-Ritzi; Mlynek, J.; Elbs, H.; Krausch, G. *Macromolecules* **1997**, *30*, 4945.
(41) Kielbassa, S.; Kinne, M.; Behm, R. J. *J. Phys. Chem. B* **2004**, *108*, 19184.

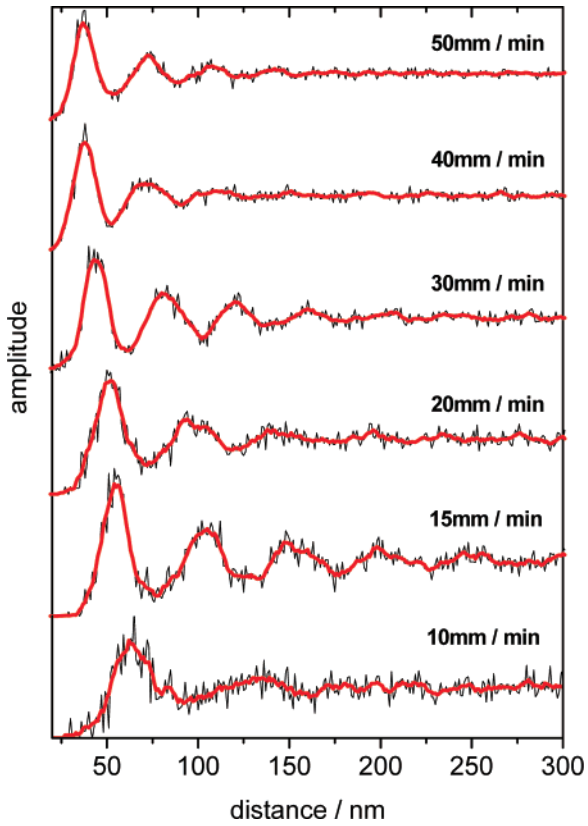

Figure 2. Pair correlation function taken from SEM images for dip-coating velocities between 10 mm min^{-1} and 50 mm min^{-1} (deposition temperature 20 °C). The amplitude has been normalized to unity at higher distances (black solid line: original data, red solid line: numerically smoothed curve).

the fully oxidized, dielectric bulk TiO_2 substrate, significant charging during SEM imaging decreased the quality of the SEM images in Figure 1, they reveal a systematic trend of a decreasing interparticle spacing with rising emersion velocity. The interparticle distance was obtained from the pair correlation function (for details see the Experimental Section). The pair correlation functions were averaged over several images taken on the same sample at macroscopic distances (mm). The corresponding results are depicted in Figure 2 which compares the pair correlation functions obtained for different emersion velocities. Although all curves show more or less pronounced oscillations at short distances, reflecting the local short-range order, at larger distances these oscillations decay and approach unity. Taking the position of the first maximum as a measure for the nearest neighbor distance, these curves reproduce the trend of a decreasing interparticle distance, with the average distance between neighboring particles decreasing by nearly a factor of 2 from about 61 nm interparticle distance at 10 mm min^{-1} to 37 nm at the highest emersion velocity. This is equivalent to an increase in particle density by nearly a factor of 4.

The degree of order in the particle adlayer is illustrated by the number of oscillations visible and by the decay of the amplitudes with increasing distance, compared to the first maximum describing the nearest neighbor shell. Nonvanishing oscillations at higher distances are indicative for the presence of a pronounced medium-range order in the corresponding array. These are clearly present for emersion velocities between 15 and 30 mm min^{-1}, whereas for very low (10 mm min^{-1}) and very large emersion velocities (40−50 mm min^{-1}), the rapid decay of the oscillations amplitudes reflects a rather poor order of the resulting nanoparticle arrays.

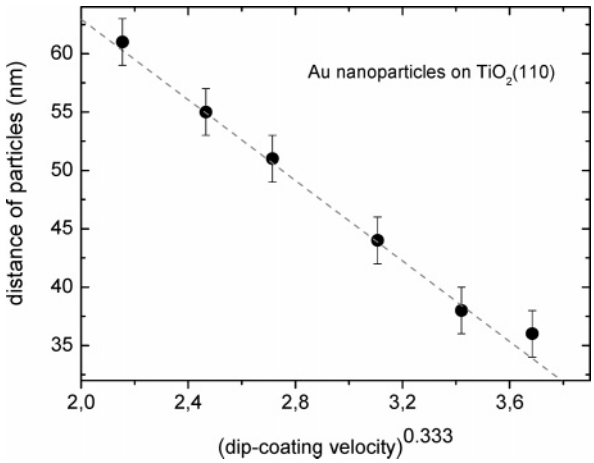

Figure 3. Interparticle distance (full symbols) displayed as a function of the third root of the dip-coating velocity. The dashed curve represents a straight line fitted to the data.

The nearest neighbor distances extracted from Figure 2 are plotted as function of the emersion velocity U in Figure 3. These experimental data can be well described by a $U^{1/3}$ behavior (dashed line), thereby supporting a model for dip-coating processes proposed earlier, where the thickness of the resulting film after emersion was related to the physical properties of the liquid such as viscosity or surface tension.[42,43] Within that model, the maximum thickness h_∞ of a wetting film on a substrate after removal from a liquid (in our case: the micellar solution with toluene as solvent) can be correlated to the capillary number Ca, the surface tension σ and the density ρ by the following equation:

$$h_\infty = 0.946 \cdot \sqrt{\frac{\sigma}{\rho g}} \mathrm{Ca}^{2/3}$$

where g denotes the standard acceleration of gravity. This relation is only valid if the capillary number $\mathrm{Ca} = \mu U/\sigma$, with μ representing the dynamic viscosity, is small compared to unity.[44] This condition is clearly fulfilled for our system, since the capillary number can be estimated to about 3.7×10^{-6} (toluene: $\rho =$ 0.857 g cm^{-3} at 20 °C, $\sigma = 0.027$ N m^{-1} at 25 °C, $\mu = 0.6$ mPa s at 20 °C). Consequently, the maximum thickness h_∞ of the liquid film should be related to the emersion velocity U by the following power law:

$$h_\infty \propto U^{2/3}$$

Assuming a constant concentration of micelles in the solution, h_∞ should also be proportional to the number of deposited micelles per unit area after evaporation of the solvent. Thus, for a monomicellar film on the substrate after drying, the areal density of micelles should also be proportional to $U^{2/3}$, leading to an interparticle distance proportional to $U^{1/3}$ as observed in our experiment.

The formation of well-ordered (two-dimensional) arrays of nanoparticles from particle solutions has been described as a delicate balance between attractive capillary forces between neighboring nanoparticles (within the liquid film) and repulsive forces due to electrostatic or steric interactions, taking into account also the evaporation of the solvent from the emersed part of the surface.[45] For a more detailed discussion see refs 45−47.

(42) Landau, L. D.; Levich, B. *Acta Physicochem. U.R.S.S.* **1942**, *17*, 42.
(43) Darhuber, A. A.; Troian, S. M.; Davis, J. M.; Miller, S. M.; Wagner, S. *J. Appl. Phys.* **2000,** *88*, 5119.
(44) Wilson, S. D. R. *J. Eng. Math.* **1982**, *16*, 209.
(45) Dimitrov, A. S.; Nagayama, K. *Langmuir* **1996**, *12*, 1303.

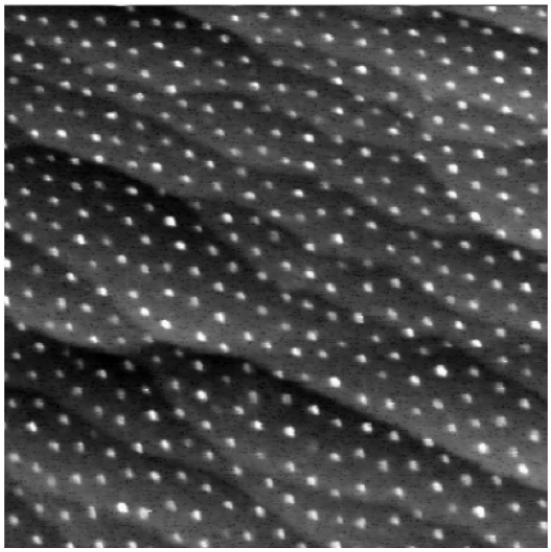

Figure 4. Noncontact AFM image of Au nanoparticles prepared by the micellar technique on TiO_2(110) applying a dip-coating velocity of 4 mm min^{-1} (image size: 800 nm × 800 nm).

The effect of the polymer size is demonstrated by changing the diblock-copolymer from PS[528]-*b*-P2VP[177] to PS[312]-*b*-P2VP[74]. Whereas, in the first case, no medium-range order was obtained for emersion velocities below 8 mm min^{-1}, this is different for the smaller polymer. Here, adlayers with a high degree of hexagonal order can be obtained at 4 mm min^{-1}, as shown in the noncontact mode AFM image in Figure 4 obtained in UHV conditions. Hence, with decreasing molecular weight of the diblock copolymers, the optimum emersion velocity for obtaining well-ordered mono-micellar films (and, thus, well-ordered nanoparticle arrays) decreases, which agrees well with earlier findings for noncommercial, optimized copolymers.[48]

The effect of the substrate is demonstrated by changing from a TiO_2(110) substrate to a silicon wafer covered by a thin layer of native silicon oxide, while maintaining all other parameters of the preparation cycle and using the same copolymers as applied for the experiments depicted in Figures 1−3 (PS[528]-*b*-P2VP-[177]). The adlayer order obtained for this material combination and an emersion velocity of 14.5 mm min^{-1} is illustrated in the SEM image (upper panel) and the corresponding pair correlation function (lower panel) in Figure 5. (Note that the quality of the SEM images is much better than in Figure 1 because of the significantly higher electrical conductivity of doped silicon compared to TiO_2.) Compared to the titania substrate, the degree of order is clearly improved as indicated by the high number of oscillations and their amplitude. Furthermore, the interparticle distance is significantly decreased on the Si/SiO_2 substrate, from approximately 52 (titania) to 37 nm (silica), while keeping all other experimental conditions unchanged. Thus, interactions between the toluene film and the substrate and, possibly, between the micelles and the substrate, which are not included in the model presented before, seem to play a decisive role for the resulting inter-particle spacing.

A similar increase in particle density with increasing emersion velocity as described above (Figure 1) was observed also for the deposition of Au salt loaded micelles on a SiO_2 substrate. This

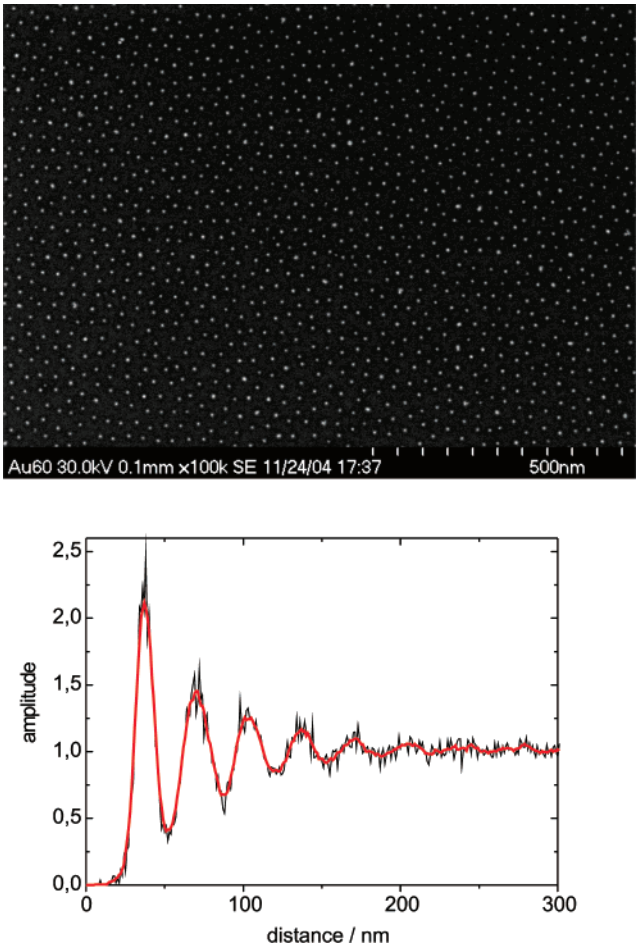

Figure 5. Upper part: SEM image of Au nanoparticles on a Si wafer after polymer removal, with identical diblock-copolymers as those used for the samples in Figure 1. Dip-coating velocity: 14.5 mm. Lower part: corresponding pair correlation (black solid line: original data, red solid line: numerically smoothed curve).

is illustrated in the SEM images in Figure 6. Note that in this case the polymer was not removed, and thus, the individual objects are much larger in diameter than in Figure 1. Similar to Figure 1, the density of the particles increases with the emersion velocity. The related pair correlation functions, which are presented in Figure 7, show a similar type of damped oscillations as observed in the pair correlation curves in Figure 2 and a similar decrease in nearest neighbor distance with increasing emersion velocity, from 110 nm at 2 mm min^{-1} to 62 nm at 31 mm min^{-1}. Because of the different polymer used here (PS[1779]-*b*-P2VP[857]), which is much larger than that used in Figure 1, the particle densities are significantly lower than in Figure 1 for similar emersion velocities. On an absolute scale, the polymer effect overcompensates the expected increase in particle density when changing from a titania to a silica substrate (see above). The highest degree of order is reached again at about 15 mm min^{-1}; at higher as well as lower velocities, the amplitudes of the oscillations are less pronounced. The interparticle distances on SiO_2 exhibit a similar linear relation versus $U^{1/3}$ as observed before on TiO_2 (Figure 3). In total, going to another polymer and another substrate does not affect the general trends, but the conditions for optimum order and the resulting particle separations will differ.

Finally, we systematically investigated the influence of the temperature on the dip coating process. The temperature may affect this process in several ways. First of all, the temperature will affect the physical properties of the solvent such as density,

(46) Potemkin, I.; Kramarenko, E. Y.; Khokhlov, A. R.; Winkler, R. G.; Reineker, P.; Eibeck, P.; Spatz, J. P.; Möller, M. M. *Langmuir* **1999**, *15*, 7290.
(47) Spatz, J. P.; Eibeck, P.; Mössmer, S.; Möller, M. M.; Kramarenko, E. Y.; Khalatur, P. G.; Potemkin, I.; Khokhlov, A. R.; Winkler, R. G.; Reineker, P. *Macromolecules* **2000**, *15*, 150.
(48) Hartmann, C., Ph.D. Thesis, Ulm University: Ulm, Germany, 2003.

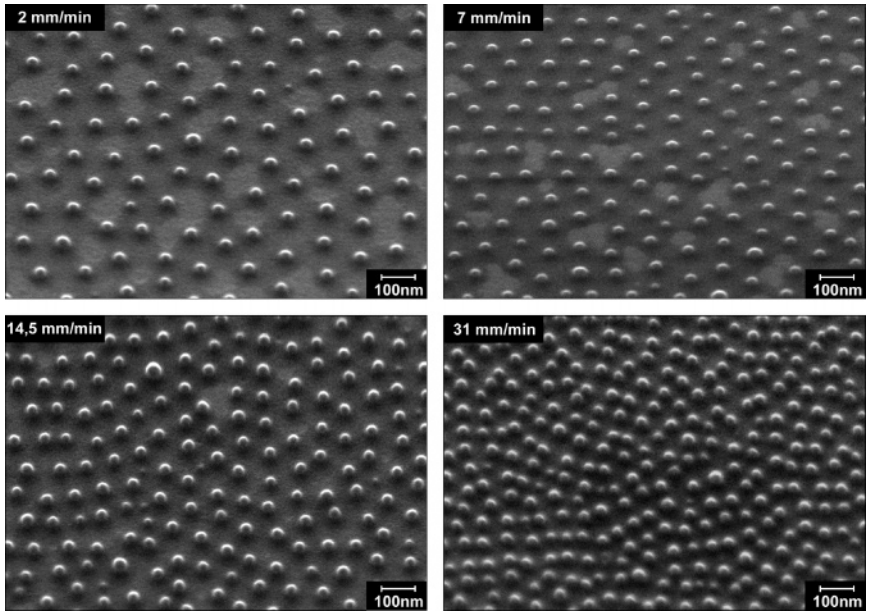

Figure 6. SEM images taken from Au-salt loaded micelles on a Si wafer with PS[1779]-b-P2VP[857] diblock-copolymers. The dip-coating velocity during deposition at 20 °C has been varied: (a) 2, (b) 7, (c) 14.5, and (d) 31 mm min^{-1}.

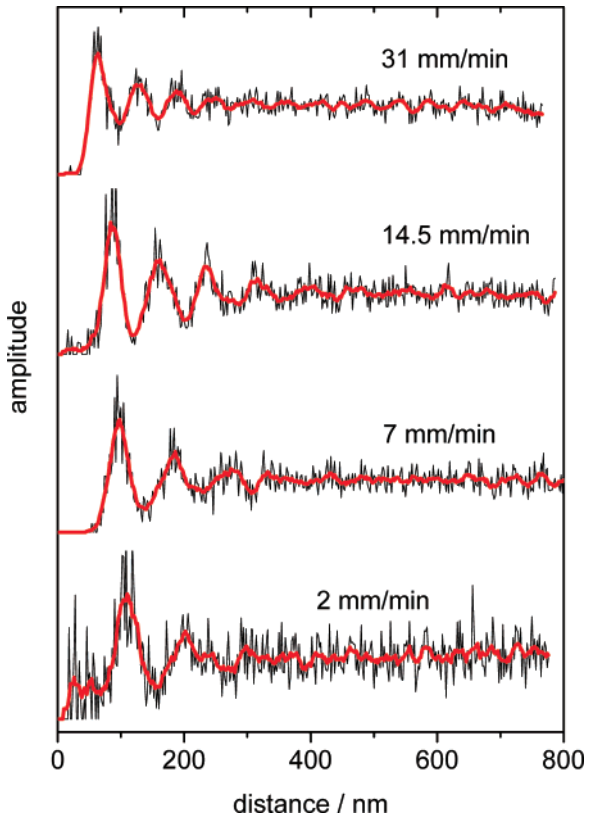

Figure 7. Pair correlation of Au micelles on a Si wafer calculated from SEM images for dip-coating velocities between 2 and 31 mm min^{-1} (black solid line: original data, red solid line: numerically smoothed curve).

viscosity, surface tension, and interface tension toward the oxide substrate, which in turn will affect the thickness of the film during emersion (film coating model). Second, deposition of colloidal particle systems that can be approximated by hard spheres generally leads to a significantly improved hexagonal order as compared to soft micellar systems.[45,49,50] Thus, lowering the deposition temperature could help to improve the quality of the micellar arrays by "hardening" the polymer chains forming the micelles. Third, an increased temperature during deposition could also help to improve the order by an increased mobility of the micelles on the substrate especially when maintaining a toluene atmosphere during and after the dip-coating process. In this case, the micelles are expected to better find their equilibrium positions on the substrate while still being mobile in the liquid toluene film. In contrast to this kinetic effect, an increased temperature may also lead to an increased disorder due to thermal excitation, and finally, higher temperatures may ultimately also result in micelle decomposition.

For studying these possible effects, Au-salt loaded micelles were deposited on Si/SiO_2 substrates at different temperatures at a constant emersion speed (15 mm min^{-1}) and subsequent relaxation in a toluene saturated atmosphere for 5 min in all cases. The polymer and the other experimental conditions are identical to those used for the experiments presented in Figure 6. The corresponding results are presented in Figure 8 which shows a series of SEM images taken after deposition at temperatures between approximately 50 (a) and 14 °C (d). The images lead to the following conclusions: (i) A hexagonal short-range order only exists for temperatures up to 32 °C; at about 50 °C the order is completely lost, which may be related to a decomposition of the micelles. (ii) At temperatures lower than room temperature, the micellar film is no longer continuous. Several regions on the substrate are free of particles, as shown in Figure 8d obtained at 14 °C, or even more pronounced, at 1 °C (SEM image not shown). (iii) The inter-particle distance is increased when rising the temperature from 20 to 32 °C. For a more detailed analysis, the pair correlation function is shown in Figure 9 for temperatures between 1 (bottom curve) and 50 °C (topmost curve). For deposition at about 50 °C, the curve indicates a complete loss of order (see also the SEM image in Figure 8a). At 32 °C, the distance between neighboring micelles increases to 108 nm as compared to approximately 76 nm obtained at room temperature (20 °C). (The slightly different value of 76 nm (Figure 8c) compared to nearest neighbor distance of 84 nm in Figure 6c, which was observed for the same diblock copolymer

(49) Kiely, C. J.; Fink, J.; Brust, M.; Bethell, D.; Schiffrin, D. J. *Nature* **1998**, *369*, 444.

(50) Sun, S.; Murray, C. B.; Weller, D.; Folks, L.; Moser, A. *Science* **2000**, *289*, 1989.

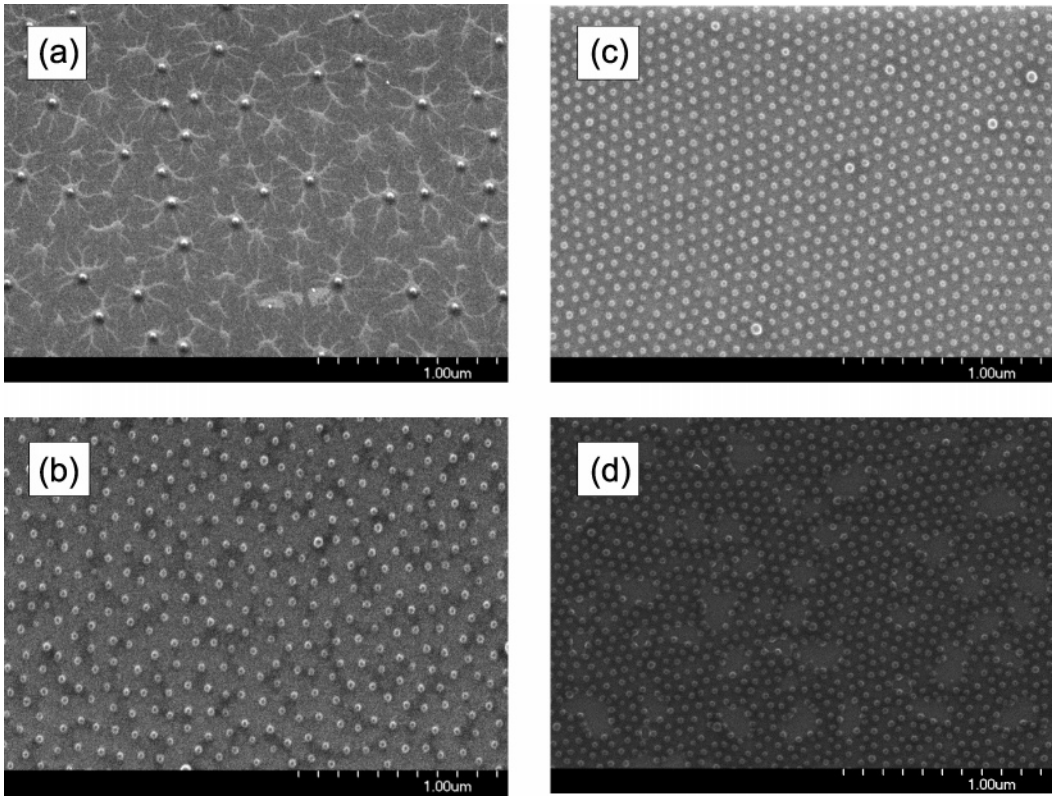

Figure 8. SEM images taken from Au-salt loaded micelles on a Si wafer at constant dip-coating velocity (15 mm min^{-1}), but different temperature; (a) ~50, (b) 32, (c) 20, and (d) 14 °C.

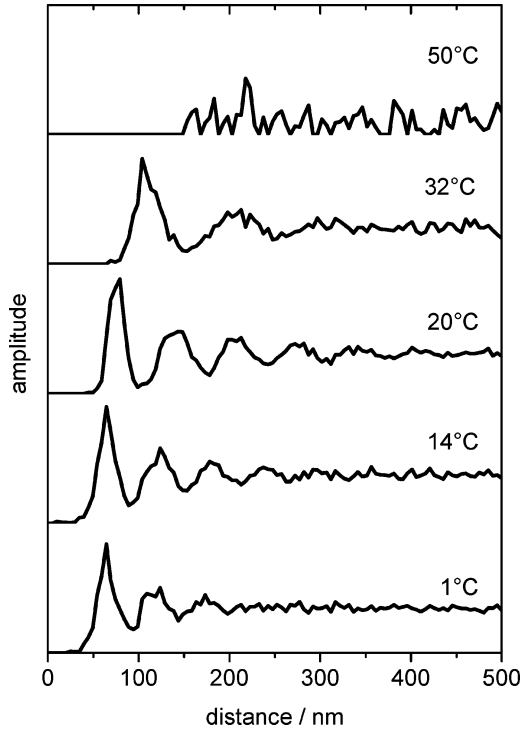

Figure 9. Pair correlation function of Au-salt loaded micelles on a Si substrate surface taken from SEM images for temperatures between 1 and 50 °C (dip-coating velocity: 15 mm min^{-1}).

and identical experimental parameters, is within the experimental uncertainty.) Upon further lowering the temperature to 1 °C, the interparticle distance further decreases. In total, the trend in this sequence agrees fully with expectations based on the temperature dependent changes in viscosity, density and surface tension, and the resulting change in film thickness with temperature. At temperatures below room temperature, toluene starts to de-wet, resulting the particle free areas on the surface at 14 and 1 °C.

Overall, well ordered adlayer structures, with a high degree of hexagonal order, could only be obtained in a narrow temperature regime between 20 and 32 °C (Figure 8b,c), i.e., at or around room temperature, which has been the standard approach in our previous experiments.[18,27−31,33,51]

4. Conclusions

We have shown that the degree of order and the interparticle distance in micellar adlayers obtained upon dip-coating deposition of Au-salt loaded micelles on oxide surfaces depends sensitively on the emersion velocity and, less pronounced, on the deposition temperature, and on the nature of the substrate material. For identical materials and other parameters, the distance between neighboring micelles can be varied within a certain range in a controlled way by changing the emersions speed U, with the resulting micelle density being proportional to $U^{2/3}$. This allows the controlled modification of the interparticle spacing in nanostructured surfaces consisting of otherwise identical nanoparticles deposited on oxide substrates, by deposition of metal loaded micelles and subsequent plasma-induced removal of the polymer.

Acknowledgment. We thank J. Schnaidt for assistance in the measurements and P. Walther for his continuous support in scanning electron microscopy. Financial support by the Deutsche Forschungsgemeinschaft (DFG) within the Collaborative Research Center (SFB) 569 is gratefully acknowledged.

LA7012304

(51) Boyen, H.-G.; Kästle, G.; Weigl, F.; Koslowski, B.; Dietrich, C.; Ziemann, P.; Spatz, J. P.; Riethmüller, S.; Hartmann, C.; Möller, M.; Schmid, G.; Garnier, M. G.; Oelhafen, P. *Science* **2002**, *297*, 1533.